The Temporal Evolution of Convective Indices in Storm-Producing Environments

TIMOTHY J. WAGNER, WAYNE F. FELTZ, AND STEVEN A. ACKERMAN

Cooperative Institute for Meteorological Satellite Studies, University of Wisconsin—Madison, Madison, Wisconsin

(Manuscript received 21 May 2007, in final form 1 February 2008)

ABSTRACT

Temporal changes in stability and shear associated with the development of thunderstorms are quantified using the enhanced temporal resolution of combined Atmospheric Emitted Radiance Interferometer (AERI) thermodynamic profile retrievals and National Oceanic and Atmospheric Administration (NOAA) 404-MHz wind profiler observations. From 1999 to 2003, AERI systems were collocated with NOAA wind profilers at five sites in the southern Great Plains of the United States, creating a near-continuous dataset of atmospheric soundings in both the prestorm and poststorm environments with a temporal resolution of up to 10 min between observations.

Median values for several standard severe weather indices were calculated for tornadic storms and nontornadic supercells. It was found that instability generally increases throughout the preconvective period, reaching a peak roughly 1 h before a tornado forms or a nontornadic supercell forms large hail. Wind shear for both tornadic and nontornadic storms starts to increase roughly 3 h before storm time. However, indices are highly variable between time and space and may not be representative of the environment at large.

1. Introduction

Showalter (1953) introduced convective indices to characterize the ability of the environment to support convection. Many climatologies of the convective stability of environments associated with the development of certain types of storms (e.g., Brooks et al. 1994; Rasmussen and Blanchard 1998) are based upon in situ profiles taken with rawinsondes launched at the synoptic times of 0000 and 1200 UTC. Only one observation time per storm is used in the calculation of these statistics due to the 12-h temporal resolution of the observations, making it difficult to investigate the evolution of preconvective environmental stability and shear using rawinsondes alone. Similarly, monitoring stability changes during the lengthy interval between rawinsonde launches is a challenge for operational forecasters (Johns and Doswell 1992; Moller 2001). Instead of rawinsondes, Thompson et al. (2003) used supercell proximity soundings modeled by the Rapid Update Cycle-2 (RUC-2) numerical weather prediction model (Benjamin et al. 1998) to create a climatology of convective indices by storm type, but as only one model sounding per storm was used, the evolution of environmental convective indices throughout the storm life cycle was not investigated.

Ground-based remotely sensed observations can provide a nearly continuous series of observations of temperature, moisture, and wind profiles. Observations of the lower troposphere are available at a temporal resolution of better than 10 min by combining the physical temperature and moisture retrievals obtained from radiance observations of the Atmospheric Emitted Radiance Interferometer (AERI; Knuteson et al. 2004a,b) with wind vector observations from the National Oceanic and Atmospheric Administration (NOAA) Profiling Network (NPN).

From late 1999 through 2003, AERI instruments were placed at or near five NPN sites in Oklahoma and Kansas as part of the U.S. Department of Energy (DOE) Atmospheric Radiation Measurement (ARM) program (Stokes and Schwartz 1994). Four of the AERI units were located on site of the NPN installation; the fifth was separated by 20 km. With 4 yr of near-continuous data observed by this array of observation sites in the southern Great Plains (SGP) of the continental United States, where severe convective activity is common, aggregate statistics of trends in atmospheric stability and shear can be analyzed.

Corresponding author address: Timothy J. Wagner, CIMSS, 1225 W. Dayton St., Madison, WI 53706.
E-mail: tjwagner2@wisc.edu

DOI: 10.1175/2008WAF2007046.1

2. Instrumentation overview

a. AERI

AERI is an accurately calibrated ground-based interferometer that measures downwelling infrared thermal emissions from the atmosphere. It has a spectral resolution of better than one wavenumber over the interval of 550–3300 cm^{-1} (18–3 μm). During the course of its 7-min observation cycle, AERI records an atmospheric spectrum and calibrates itself against two blackbodies obtaining a radiometric accuracy of better than 1% ambient radiance and reproducibility of better than 0.2%. It is automated and field-hardened; diagnostic checkups can be completed remotely, making it suitable for installation in a variety of harsh environments.

Profiles of temperature and moisture can be obtained from AERI-observed spectra through a combined statistical and physical retrieval. A brief outline of the AERI retrieval algorithm is presented here; further details can be found in the literature (Smith et al. 1999; Feltz et al. 1998, 2005).

In the retrieval process, a first guess for a valid profile is formed by blending output from the RUC-2 numerical weather prediction model with statistical regressions of radiances obtained from using a radiative transfer model on clear-sky rawinsonde profiles of temperature and moisture. The RUC-2 four-dimensional gridded data are interpolated in time and space to obtain a profile of the atmospheric state that coincides with the AERI observation while the finer vertical resolution of the statistical regressions is used in the lower atmosphere where finer-scale phenomena like inversions are present. This first guess is then processed through a forward radiative transfer model along with surface observations of temperature and moisture to convert the first-guess profile into a radiative spectrum that is then compared with the observed AERI spectrum. The modeled spectrum is then adjusted to minimize the difference between the modeled and observed radiances and the cycle iterates until the resulting profile has radiance measurements within a specified tolerance of the AERI observation. Since clouds and precipitation are infrared emitters, retrievals are only possible when skies are clear or clouds are high. Data taken from a laser ceilometer are ingested into the algorithm to ensure that these conditions are met. AERI-retrieved profiles show good agreement with rawinsonde thermodynamic profile and stability observations (Feltz et al. 2003a,b; Feltz and Mecikalski 2002; Turner et al. 2000).

b. NOAA Profiling Network

The NPN consists of 32 sites in the continental United States plus three in Alaska. The radar wind profilers (Chadwick and Hassel 1987) operate at a frequency of 404.37 MHz, using a fixed phased-array coaxial–colinear grid antenna. An NPN radar consists of three beams: one pointing vertically and two others pointing north and east at an elevation angle of 73.7°. By observing reflectivity gradients in the clear air, the radar is able to generate a three-dimensional profile of wind vectors. The radar profiler samples in two modes: low- and high-altitude mode; the boundary between the two modes is at 7.5 km above ground level (AGL). No observations higher than 6 km in altitude are used in this study; therefore, all observations come from the low-altitude mode, which has a 250-m vertical resolution.

NPN observations are currently taken every 6 min. As with AERI dwell time, this allows for frequent sampling while allowing enough time for averaging to reduce some of the noise. Radar wind profilers show good agreement with rawinsonde observations. Bedka et al. (2006) compared over 700 rawinsondes launched from the ARM SGP Central Facility in Lamont, Oklahoma, and found the profiler wind speed RMS error for the 6-min resolution observations was 2.43 m s^{-1} with a bias of -0.19 m s^{-1}.

3. Methodology

To help determine that the majority of prestorm observations were representative of the inflow region of a developing storm, the storms evaluated in this study were located within a radius of 200 km of an AERI site and within an angle of $\pm 75°$ downwind of the mean surface wind vector during the 6 h prior to storm time.

The SeverePlot database (Hart 1993) was used to determine the times and locations of severe weather events. NOAA's Storm Prediction Center (SPC) maintains this database of tornadoes, severe wind, and severe hail, and it is accessible through a graphical interface. SeverePlot includes the times, dates, latitudes, longitudes, and magnitudes of these severe weather events, and was used to locate all reported tornadoes that initially formed in the southern Great Plains during the 4-yr period of AERI deployment. If multiple tornadoes formed within 6 h of each other and were observed by the same AERI site, only the first tornado was included in the statistical analysis presented here; if treated separately, two tornadoes occurring in the range of the same observation site within a short time span would return almost identical observations and improperly bias the statistical analysis. A map of the locations of the AERI sites as well as the storms investigated in this study is shown in Fig. 1.

Stability and shear indices were calculated for the remaining tornadic events using the combined AERI

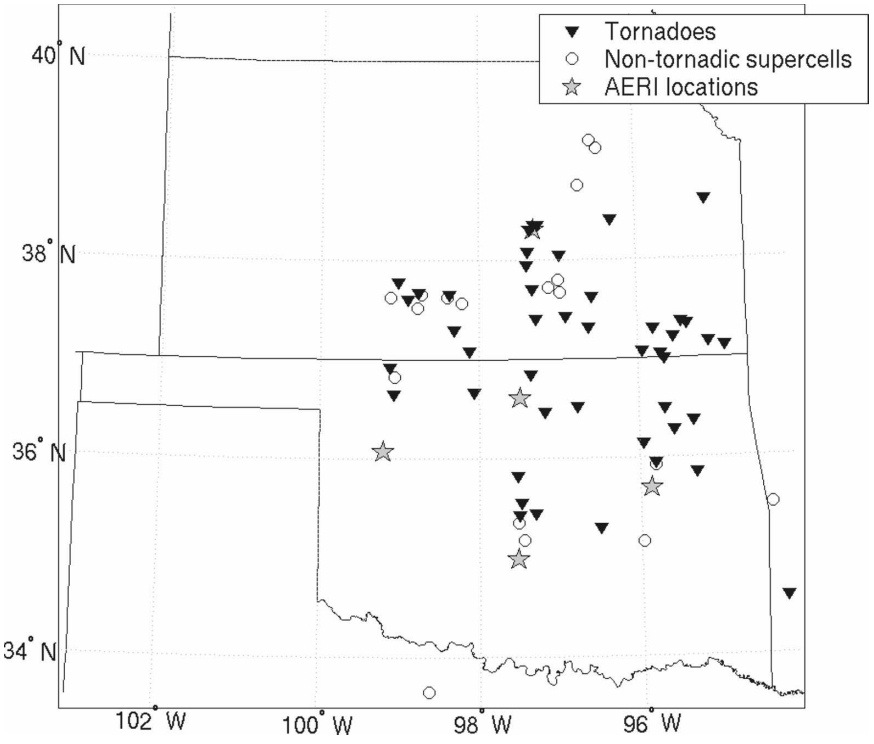

FIG. 1. Map of the experiment domain. Shown are the locations of tornadoes and supercells used in this study (black triangles and white circles, respectively), as well as the five AERI installations (shaded stars).

and NPN observations. Observations from these ground-based instruments are not always continuous, however. AERIPROF (Feltz et al. 2005), the AERI profile retrieval algorithm, will reject observations when low clouds are present and AERI automatically closes its optics hatch when precipitation is detected, making observations impossible during those times. The AERI profiles used in this study were augmented with the RUC-2 first-guess profile when thermodynamic retrievals were not possible due to these conditions. As a result of this procedure, different storm types are typically analyzed with different datasets depending on the environment in which they form. Tornadoes that develop from supercells are more likely to be observed by AERI, while tornadoes that are generated by quasi-linear systems or other environments with substantial cloud cover must be analyzed with RUC-2 data. Storms occurring prior to March 2002 are analyzed with hourly NPN data instead of 6-min data as the finer-resolution data are not available through the ARM data archive.

Nontornadic supercells remain an active area of study, in part to determine why some storms that seem potentially tornadic do not form tornadoes. Since the SeverePlot database does not contain a list of these storms, such a dataset had to be created from other observations. For this study, a nontornadic supercell was considered to be a storm that produced hail of 5 cm (2 in.) or larger and was separated from a tornado by more than 6 h. This hail diameter criterion was introduced by Rasmussen and Blanchard (1998) under the assumption that only rotating updrafts would be large enough to support hail of that size. Thompson et al. (2003) found that 90% of the 5 cm or larger hail reports could be linked to supercells. As many tornadic storms produce hail, the temporal separation requirement is necessary to prevent classifying environments that are capable of producing both tornadic and nontornadic storms as purely nontornadic. Issues are raised with this methodology, however. While a tornadic storm clearly has a time of definition associated with it, the time at which a storm can definitively be labeled as a nontornadic supercell is less clear as proxy evidence can accurately determine neither the time that updraft rotation begins nor the time that tornado formation is no longer possible for a particular storm. For this study, the time associated with a nontornadic storm merely represents the earliest report of hail greater than or equal to 5 cm in diameter. In light of this, this study uses the term "event time" to represent the time when a storm is defined as a tornadic or nontornadic event. The same criteria for deleting multiple tornadoes were ap-

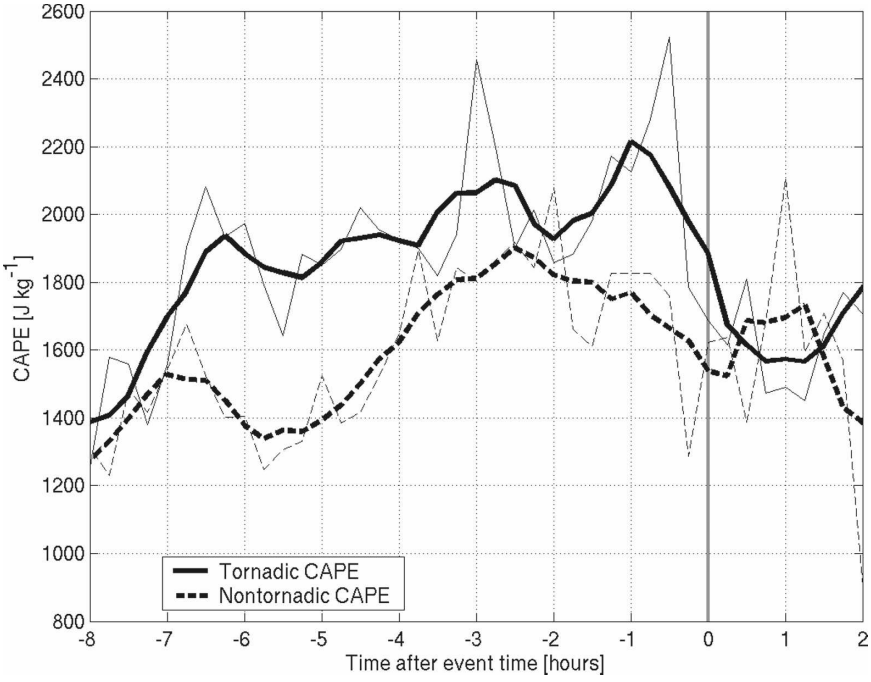

FIG. 2. Plot of median values of CAPE as derived from AERI-retrieved thermodynamic profiles for tornadic storms (solid line) and nontornadic storms (dashed line) from 8 h before storm formation to 2 h after storm formation. The 1-h running mean is highlighted as the thick line; the thin line is without the running mean applied.

plied to supercells, and thenceforth the same procedures for index calculation and interpolation were used. These procedures resulted in 46 tornadic events and 18 nontornadic events used as the basis for this study. The median event time for the storms used in this study was 0003 UTC for tornadic events and 0043 UTC for nontornadic events. Thus, the aggregate evolutions of environments for both storm types contain similar diurnal forcing.

4. Results

All convective indices that were calculated for this study were adjusted to a common temporal grid encompassing 8 h before event time to 2 h after in order to assess the evolution of the environment throughout the life cycle of the storm. The median value of an index for each time step for all storms of a given type was then calculated. Running means of 1 h were calculated to reduce noise and aid in the assessment of trend evolution.

Variability is large in the values of convective indices for these storms, both in comparison from one storm to another as well as from one observation time to the next within an individual storm. Indices are highly dependent on the measured values of the thermodynamics and kinematics in the lowest levels of a profile. Small fluctuations in low-level moisture and boundary layer winds will cause significant change from one time step to the next. As AERI weighting functions peak close to the surface, the highest vertical resolution in the thermodynamic profiles used in this study is found where the observations have the most impact on calculated indices, contributing to the observations of large temporal variability.

For tornadic storm environments, the median value of the convective available potential energy (CAPE; Moncrieff and Green 1972) shows a gradual trend of increasing instability until 1 h before tornadogenesis (Fig. 2), reaching a peak of over 2200 J kg^{-1}. The CAPE then drops off quickly until tornadogenesis, after which it continues to decrease at a slower rate. Nontornadic supercell environments exhibit a slightly different behavior; the median value of CAPE exhibits a faster increase than the median tornadic environment CAPE, rising from around 1300 J kg^{-1} at 6 h before event time to a peak of over 2000 J kg^{-1} at 2 h before event time, a value slightly larger than the CAPE value for tornadic storms at that time. This is followed by a prolonged reduction of CAPE. During the postevent time domain, the median tornadic CAPE exhibits slightly more constant behavior than nontornadic CAPE. All CAPE values presented here are most unstable CAPE (muCAPE), and the virtual temperature correction (Doswell and Rasmussen 1994) was applied.

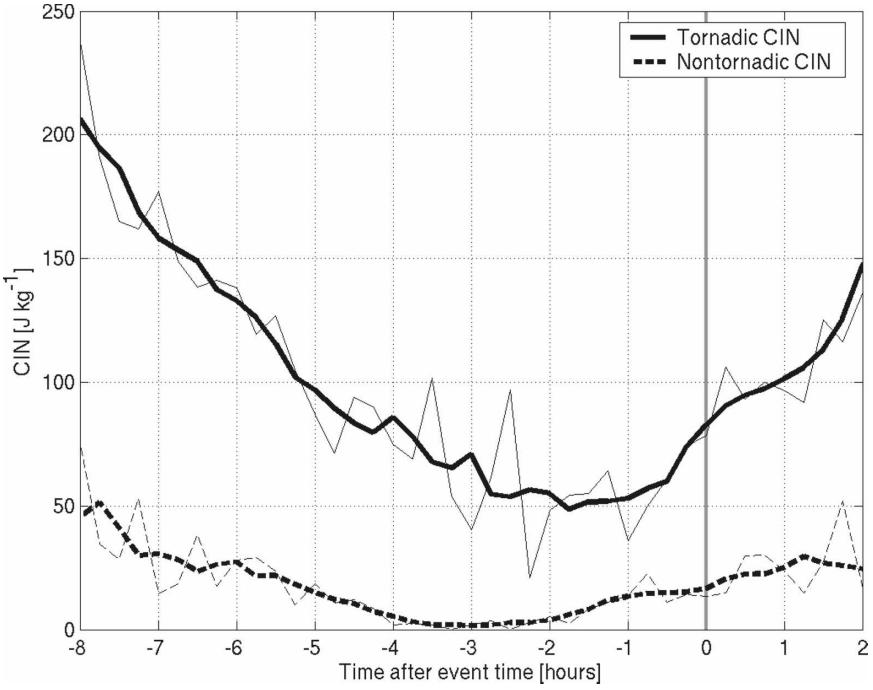

FIG. 3. As in Fig. 2, but for CIN.

The median value of convective inhibition (CIN; Fig. 3) is larger for tornadic environments than it is for nontornadic supercell environments throughout the storm development cycle. The quantity of least median CIN in both tornadic and nontornadic environments is found between 2 and 4 h prior to event time, with the median tornadic CIN reaching a brief minimum of 20 J kg^{-1} with a running mean near 50 J kg^{-1} and median nontornadic CIN reaching a minimum of less than 5 J kg^{-1}. Outside of the time of minimum median values between 2 and 4 h prior to event time, median tornadic CIN is roughly 5 times the median nontornadic CIN throughout the storm formation cycle.

Just as thermodynamic indices are used to quantify convective instability present in the environment, kinematic indices can be used to quantify the amount of wind shear. One of the most common measurements of wind shear is storm-relative helicity (SRH; Davies-Jones et al. 1990). Environments with large levels of SRH have been shown to support longer-lived storms than those that form in environments with lesser levels of SRH (Droegemeier et al. 1993). Median values of 0–3 -km storm-relative helicity can be calculated by using the wind profiles measured by NPN and applying a storm motion parameterization to obtain the required storm-relative wind speeds. To assess storm motion from a single observation point, the Bunkers scheme is used (Bunkers et al. 2000), in which the storm motion of a right-moving supercell ($\mathbf{V}_{RM}$) is

$$\mathbf{V}_{RM} = \mathbf{V}_{mean} - D\left[\frac{\mathbf{V}_{shear} \times \mathbf{k}}{(\mathbf{V}_{shear})}\right], \quad (1)$$

where $\mathbf{V}_{mean}$ is the 0–6-km mean wind vector, D is the deviation of the mean wind vector of 7.5 m s^{-1}, and $\mathbf{V}_{shear}$ is the vertical wind shear vector. The results from the NPN sites in the SGP show that the median value of the tornadic environment SRH is mostly constant in the hours before tornadogenesis, staying between 225 and 250 m^2 s^{-2} until tornado formation is imminent (Fig. 4). From 1 h before event time to 2 h after, the median value of tornadic SRH increases linearly with time, at the rate of 40 m^2 s^{-2} h^{-1}. From 6 h prior to event time to 0.5 h prior to event time, the median nontornadic SRH is less than the tornadic SRH. Median nontornadic SRH also exhibits a slightly faster linear increase with time, increasing by 50 m^2 s^{-2} h^{-1} from 2 h prior to event time to 2 h after.

The energy–helicity index (EHI; Hart and Korotky 1991) is calculated by combining the CAPE and 0–3-km SRH as follows:

$$\text{EHI} = \frac{\text{CAPE} \times \text{SRH}}{1.6 \times 10^5}. \quad (2)$$

Since both thermodynamic and kinematic observations are required, observations from both AERI and radar wind profilers were used to calculate EHI for this study. It was found that EHI was larger than nontornadic EHI for the 8 h preceding event time, with the biggest dif-

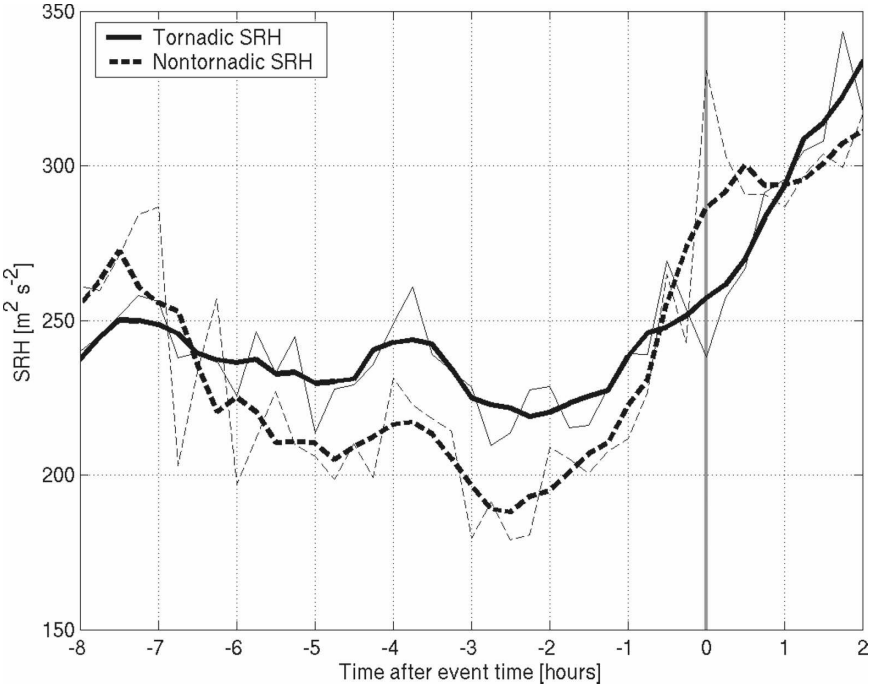

FIG. 4. As in Fig. 2, but for 0–3-km SRH as measured by NPN.

ference being between 2 and 1 hour before event time. Both tornadic and nontornadic EHIs show an increasing trend from 5.5 h before event time to 1 h before event time, at which time the tornadic EHI starts to decrease while the nontornadic EHI remains constant (Fig. 5). This mirrors the evolution of CAPE for these storm types as EHI is strongly dependent on CAPE.

Like the EHI, the bulk Richardson number (BRN; Weisman and Klemp 1982) is a combination of thermodynamic and kinematic observations. While EHI is a product of instability and shear, BRN is a ratio of the two:

$$\mathrm{BRN} = \frac{\mathrm{CAPE}}{0.5U^2}, \tag{3}$$

where U is the difference between the density-weighted mean wind vector of the lowest 6 km and the mean wind vector of the lowest 500 m. BRN is a unitless parameter as the units of CAPE and velocity squared are equivalent. The median value of BRN in tornadic environments is at its highest 5 h prior to tornadogenesis, then decreases until tornadogenesis, after which it holds steady at 25 (Fig. 6). Tornadic BRN exhibits less variability than nontornadic BRN, which could possibly mean that environments featuring highly variable values in the ratio of instability to shear are not conducive to tornado formation. Further work is needed to determine if tornadic development requires consistency in the mesocyclones formed by shear and buoyancy.

To determine the statistical significance of the differences between the tornadic and nontornadic median index values, the quartile values for the various indices were examined. Of the indices used in this study, CIN showed the largest separation between the quartiles of one storm type versus the other. Figure 7 shows the quartiles of CIN for both tornadic and nontornadic storms. The shaded region marks the overlap between the lowest quartile for tornadic CIN and the highest quartile for nontornadic CIN. The majority of the tornadic CIN values are larger than the highest quartile of the nontornadic CIN for several hours preceding event time. While elevated levels of CIN may indicate a tornadic storm instead of a nontornadic one, if CIN levels are too high, convection may be inhibited entirely. Therefore, enhanced levels of CIN alone cannot be used as a determining tornado predictor. However, it may be possible to use near–real time observations of CIN in conjunction with other indices to help determine if an environment may become tornadic.

5. Conclusions

Through active and passive observations of reflectivity and radiance, ground-based remote sensing instruments are capable of retrieving thermodynamic and kinematic profiles of the troposphere at a far finer temporal resolution than is possible with traditional rawinsonde launches. With these observations, benchmark statistics about storm environments are not lim-

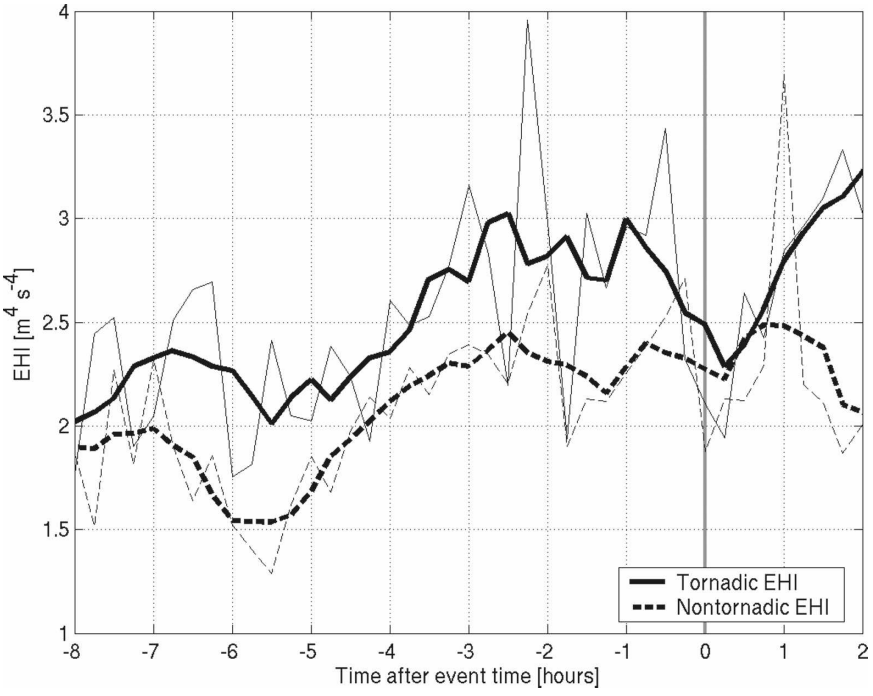

FIG. 5. As in Fig. 2, but for the energy–helicity index, measured from both AERI thermodynamic profiles and NPN wind profiles.

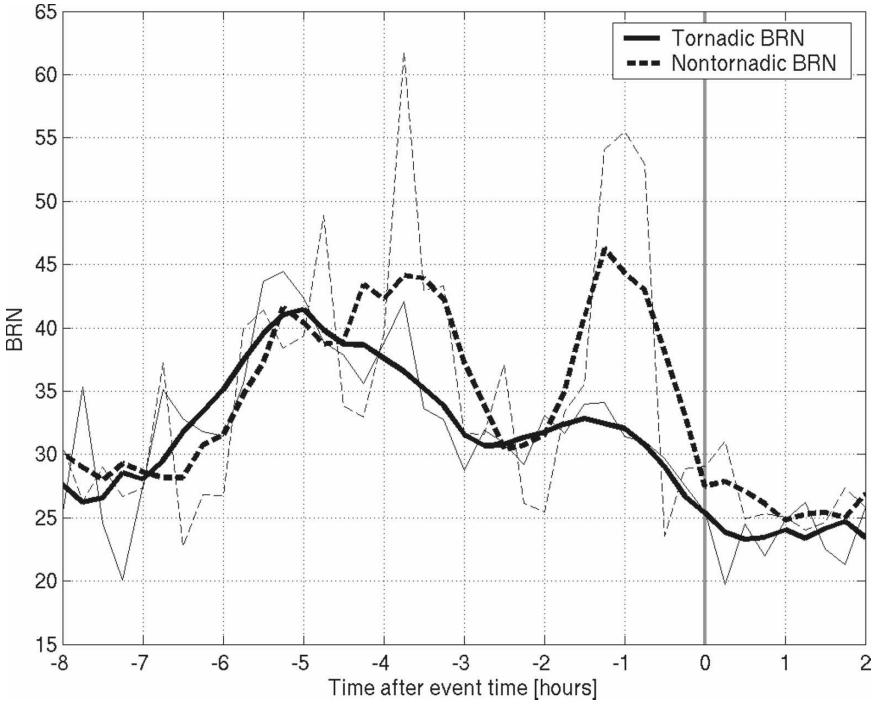

FIG. 6. As in Fig. 2, but for BRN, measured with both AERI thermodynamic profiles and NPN wind profiles.

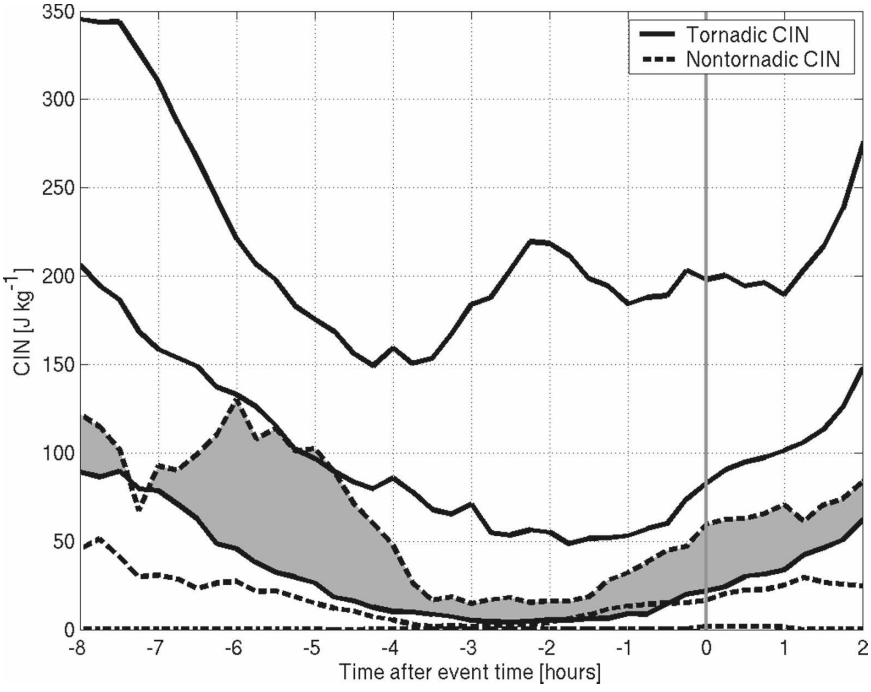

FIG. 7. Plot of the three quartile values of CIN as derived from AERI-retrieved thermodynamic profiles for both tornadic storms (solid lines) and nontornadic storms (dashed lines) from 8 h before storm formation to 2 h after storm formation. The shaded region marks the overlap between the highest quartile of nontornadic CIN and the lowest quartile of tornadic CIN.

ited to one profile per storm, but can instead trace the evolution of the near-storm environment. To quantify the thermodynamic and kinematic environments, convective indices are calculated from these remotely sensed profiles.

In the southern Great Plains of the United States, these observations show that in the range of 1–3 h before tornadogenesis, tornado-producing environments have larger levels of convective inhibition and slightly higher levels of instability than nontornadic supercell environments. The environments that produced tornadoes also had higher energy–helicity index levels throughout the entire storm development cycle than those that produced nontornadic supercells. The most significant discriminator between tornadic and nontornadic storms was convective inhibition, which was significantly higher for tornadic storms than nontornadic ones.

Values of any convective index can vary greatly from one observation time to the next due to frequent small changes in winds and low-level moisture. Convective indices calculated from an atmospheric profile are therefore highly dependent on the time and place that the profile was observed and therefore might not truly be representative of the environment at large, a phenomenon also noted by Brooks et al. (1994). While an unstable environment can clearly be discerned from a stable one, the behavior of instability is more difficult to pinpoint from a single observation obtained from a synoptic rawinsonde launch. More frequent observations, be they in the form of satellite soundings, ground-based remote sensing units, or additional balloon launches, are needed to properly capture the degree of instability present in the environment.

No obvious tornadogenesis signature was found in the time series of the traditional convective indices for the storm events used in this study. While it is possible that the spatial and temporal resolution of this remote sensing network may not yet be fine enough to resolve any signature fluctuations that may exist, the indices do not encompass all of the necessary conditions for tornadogenesis. Small-scale baroclinicity, microbursts, and microphysics may all play a role in tornadogenesis (Davies-Jones 2006). If that is the case, then the traditional convective indices, no matter how finely resolved, will be unable to perfectly characterize tornado-producing environments.

In future years, as high temporal resolution profiles from ground-based units and geostationary satellites become more common, new indices will need to be developed that take advantage of these observations by incorporating differences between observations in both

the temporal and spatial dimensions. While these new indices will not be able to replace a seasoned forecaster, they can still provide new insights and assistance to operational forecasting that are currently unresolved within the existing rawinsonde network.

Acknowledgments. The authors thank the three anonymous reviewers, whose input significantly improved this paper. Data were obtained from the Atmospheric Radiation Measurement (ARM) program sponsored by the U.S. Department of Energy, Office of Science, Office of Biological and Environmental Research, Environmental Sciences Division.

REFERENCES

Bedka, K., R. A. Petersen, W. F. Feltz, C. S. Velden, and J. R. Mecikalski, 2006: Statistical relationships between satellite-derived atmospheric motion vector, rawinsonde, and NOAA Wind Profiler Network observations. Preprints, *Seventh Int. Symp. on Tropospheric Profiling,* Boulder, CO, National Center for Atmospheric Research, 5.17. [Available online at http://www.eol.ucar.edu/istp2006/pdf/5.17A_Bedka_K.pdf.]

Benjamin, S. G., J. M. Brown, K. J. Brundage, B. E. Schwartz, T. G. Smirnova, and T. L. Smith, 1998: The operational RUC-2. Preprints, *16th Conf. on Weather Analysis and Forecasting,* Phoenix, AZ, Amer. Meteor. Soc., 249–252.

Brooks, H. E., C. A. Doswell III, and J. Cooper, 1994: On the environments of tornadic and nontornadic mesocyclones. *Wea. Forecasting,* **9,** 606–618.

Bunkers, M. J., B. A. Klimowski, J. W. Zeitler, R. L. Thompson, and M. L. Weisman, 2000: Predicting supercell motion using a new hodograph technique. *Wea. Forecasting,* **15,** 61–79.

Chadwick, R. B., and N. Hassel, 1987: Profiler: The next generation surface-based atmospheric sounding system. Preprints, *Third Int. Conf on Interactive Information and Processing Systems for Meteorology,* New Orleans, LA, Amer. Meteor. Soc., 15–21.

Davies-Jones, R. P., 2006: Tornadogenesis in supercell storms: What we know and what we don't know. Preprints, *Symp. on the Challenges of Severe Convective Storms,* Atlanta, GA, Amer. Meteor. Soc., 2.2. [Available online at http://ams.confex.com/ams/pdfpapers/104563.pdf.]

——, D. Burgess, and M. Foster, 1990: Test of helicity as a tornado forecast parameter. Preprints, *16th Conf. on Severe Local Storms,* Kananaskis Park, AB, Canada, Amer. Meteor. Soc., 588–592.

Doswell, C. A., III, and E. N. Rasmussen, 1994: The effect of neglecting the virtual temperature correction on CAPE calculations. *Wea. Forecasting,* **9,** 625–629.

Droegemeier, K. K., S. M. Lazarus, and R. Davies-Jones, 1993: The influence of helicity on numerically simulated convective storms. *Mon. Wea. Rev.,* **121,** 2005–2029.

Feltz, W. F., and J. R. Mecikalski, 2002: Monitoring high-temporal-resolution convective stability indices using the ground-based Atmospheric Emitted Radiance Interferometer (AERI) during the 3 May 1999 Oklahoma–Kansas tornado outbreak. *Wea. Forecasting,* **17,** 445–455.

——, W. L. Smith, R. O. Knuteson, H. E. Revercomb, H. M. Woolf, and H. B. Howell, 1998: Meteorological applications of temperature and water vapor retrievals from the ground-based Atmospheric Emitted Radiance Interferometer (AERI). *J. Appl. Meteor.,* **37,** 857–875.

——, H. B. Howell, R. O. Knuteson, H. M. Woolf, D. D. Turner, R. Mahon, T. D. Halther, and W. L. Smith, 2005: Retrieving temperature and moisture profiles from AERI radiance observations: AERIPROF value-added product technical description. DOE-ARM Tech. Rep. TR-066, 41 pp. [Available online at http://www.arm.gov/publications/tech_reports/arm-tr-066.pdf.]

——, D. Posselt, J. Mecikalski, G. S. Wade, and T. J. Schmit, 2003a: Rapid boundary layer water vapor transitions. *Bull. Amer. Meteor. Soc.,* **84,** 29–30.

——, W. L. Smith, H. B. Howell, R. O. Knuteson, H. Woolf, and H. E. Revercomb, 2003b: Near-continuous profiling of temperature, moisture, and atmospheric stability using the Atmospheric Emitted Radiance Interferometer (AERI). *J. Appl. Meteor.,* **42,** 584–597.

Hart, J. A., 1993: SVRPLOT: A new method of accessing and manipulating the NCCFC severe weather database. Preprints, *17th Conf. on Severe Local Storms,* St. Louis, MO, Amer. Meteor. Soc., 40–41.

——, and W. D. Korotky, 1991: The SHARP workstation v1.50: A skew T/hodograph analysis and research program for the IBM and compatible PC. NOAA/NWS Forecast Office, Charleston, WV, 62 pp.

Johns, R. H., and C. A. Doswell III, 1992: Severe local storms forecasting. *Wea. Forecasting,* **7,** 588–612.

Knuteson, R. O., and Coauthors, 2004a: Atmospheric Emitted Radiance Interferometer. Part I: Instrument design. *J. Atmos. Oceanic Tehnol.,* **21,** 1763–1776.

——, and Coauthors, 2004b: Atmospheric Emitted Radiance Interferometer. Part II: Instrument performance. *J. Atmos. Oceanic Tehnol.,* **21,** 1777–1789.

Moller, A. R., 2001. Severe local storms forecasting. *Severe Convective Storms, Meteor. Monogr*., No. 50, Amer. Meteor. Soc., 433–480.

Moncrieff, M. W., and J. S. A. Green, 1972: The propagation and transfer properties of steady convective overturning in shear. *Quart. J. Roy. Meteor. Soc.,* **98,** 336–352.

Rasmussen, E. N., and D. O. Blanchard, 1998: A baseline climatology of sounding-derived supercell and tornado forecast parameters. *Wea. Forecasting,* **13,** 1148–1164.

Showalter, A. K., 1953: A stability index for thunderstorm forecasting. *Bull. Amer. Meteor. Soc.,* **34,** 250–252.

Smith, W. L., W. F. Feltz, R. O. Knuteson, H. E. Revercomb, H. M. Woolf, and H. B. Howell, 1999: The retrieval of planetary boundary layer structure using ground-based infrared spectral radiance measurements. *J. Atmos. Oceanic Technol.,* **16,** 323–333.

Stokes, G. M., and S. E. Schwartz, 1994: The Atmospheric Radiation Measurement (ARM) program: Programmatic background and design of the Cloud and Radiation Test Bed. *Bull. Amer. Meteor. Soc.,* **75,** 1201–1221.

Thompson, R. L., R. Edwards, J. A. Hart, K. L. Elmore, and P. Markowski, 2003: Close proximity soundings within supercell environments obtained from the Rapid Update Cycle. *Wea. Forecasting,* **18,** 1243–1261.

Turner, D. D., W. F. Feltz, and R. A. Ferrare, 2000: Continuous water vapor profiles from operational ground-based active and passive remote sensors. *Bull. Amer. Meteor. Soc.,* **81,** 1301–1317.

Weisman, M. L., and J. B. Klemp, 1982: The dependence of numerically simulated convective storms on vertical wind shear and buoyancy. *Mon. Wea. Rev.,* **110,** 504–520.